Journal of Materials Chemistry B

Accepted Manuscript

ROYAL SOCIETY OF CHEMISTRY

www.rsc.org/materialsB

Zwitterionic Amphiphile Coated Magnetofluorescent Nanoparticles – Synthesis, Characterization and Tumor Cell Targeting

Violeta G. Demillo,[a,b] Xiaoshan Zhu*[a,b]

[a] *Department of Electrical and Biomedical Engineering, University of Nevada, Reno, NV, USA*

[b] *Biomedical Engineering Program, University of Nevada, Reno, NV, USA*

*To whom correspondence should be addressed. Email: xzhu@unr.edu. Phone: 1-775-682-6298. Fax: 1-775-784-6627

ABSTRACT

Magnetofluorescent nanoparticles (MFNPs) have recently attracted significant research interests due to their potential applications in biological manipulation and imaging. In this work, through a simple and fast self-assembling process, we first report the preparation of zwitterionic MFNPs (ZW-MFNPs) in the form of micelles using our newly synthesized zwitterionic amphiphiles, $CuInS_2/ZnS$ quantum dots, and $MnFe_2O_4$ magnetic nanoparticles. ZW-MFNPs integrate both $MnFe_2O_4$ magnetic nanoparticles and $CuInS_2/ZnS$ quantum dots in their hydrophobic cores and zwitterionic groups such as carboxybetaine and sulfobetaine on their hydrophilic shells. ZW-MFNPs possess dual imaging properties, high (Mn + Fe) recovery, excellent stability in aqueous solutions with a wide pH/ionic-strength range and physiological media, minimal cytotoxicity, and specific targeting to brain tumor cells after bioconjugation with chlorotoxin. The unique characteristics of ZW-MFNPs may open an avenue for these particles to be employed in broad biomedical applications.

INTRODUCTION

Magnetofluorescent nanoparticles (MFNPs) enabling simultaneous fluorescence labeling and magnetic field assisted separation, sorting, heating or imaging are gaining momentum for biomedical applications at the cellular, tissue or anatomical levels.[1-4] For this reason, many research approaches have been reported on the controlled synthesis of MFNPs regarding their size, shape, composite and surface properties.[5-20] Among them, MFNPs in the form of micelles self-assembled from amphiphilic polymers and hydrophobic magnetic nanoparticles (MNPs) and quantum dots (QDs) are very attractive.[15-20] They provide a unique core-shell structure where the

hydrophobic core is loaded with multiphase magnetofluorescent materials and the hydrophilic shell renders micelles stable in aqueous solutions. The micellar MFNPs inherit the merits of MNPs (e.g., high saturation magnetization) and QDs (e.g., photostability, luminescence wavelength tunability), and also provide complementary merits from both magnetic resonance imaging and optical imaging (i.e., high spatial resolution and high sensitivity). To achieve colloidal stability and biocompatibility for various *in vitro* or *in vivo* applications, the hydrophilic shell of this type of MFNPs are usually formed by anti-fouling poly(ethylene glycol) (PEG) chains.[16-20]

Although PEGs render MFNPs stable in physiological media,[21-22] PEGs are sensitive to solution pH and salinity and tend to cause MFNPs to aggregate in acidic or salt-rich microenvironments.[23] The aggregation will further degrade or even change the diagnosis/therapy functionalities devised for original MFNPs. This shortcoming of PEGs limits their applications in biological or biomedical experiments, where harsh conditions are ubiquitous. For instance, many cellular organelles are maintained under acidic conditions and rich in salts.[24] Moreover, recent studies suggested that PEG may induce *in vivo* production of anti-PEG immunoglobulin M (IgM) antibodies, which further affects *in vivo* applications of PEG coated MFNPs.[25-27] Overcoming the limits of PEGs, more biocompatible and hydrophilic zwitterions such as sulfobetaine and carboxybetaine are presenting as alternatives to PEGs.[23,25,28-34] Once zwitterions are coated on NP surfaces to form zwitterionic NPs, the positive and negative electrical charges in zwitterions can interact with water molecules to form a hydration layer. The hydration layer can encapsulate the NPs and prevent aggregation even in harsh conditions. Thus, it is of interest to develop zwitterion coated MFNPs or zwitterionic MFNPs (ZW-MFNPs).

To date, most of the current zwitterion-coating approaches have been developed for individual cadmium-based QDs or AuNPs.[23, 28-34] These approaches mainly involve the coupling of zwitterions with thiol ligands such as dihydrolipoic acid. These coupled ligands are further exchanged with native hydrophobic ligands (trioctylphosphine oxide) to form zwitterionic QDs through the high binding affinity of thiols to Zn or Au atoms on QD or AuNP surface. Although successful, the zwitterion coupled thiol ligands are not applicable to the preparation of MFNPs integrating both MNPs and QDs. Instead, wrapping MNPs and QDs using zwitterionic amphiphiles is a better approach to prepare ZW-MFNPs. For this purpose, the synthesis of zwitterionic amphiphiles is critical. The amphiphiles are expected to have not only zwitterions but also functional heads such as carboxyl groups for subsequent bioconjugation with biological moieties.

In this work, as illustrated in Figure 1, we propose an approach for ZW-MFNP preparation by modifying poly(maleic anhydride-alt-1-octadecene) (PMAO) to zwitterionic amphiphiles. The reason we chose PMAO is that the presence of the versatile anhydride rings on the PMAO backbone allows its structure and functionality to be tuned or modified with other functional groups. In our approach, PMAO anhydride rings are first opened by 3-(dimethylamino)-1-propylamine (DMAPA) to produce terminal tertiary amines. The tertiary amines further react with β-propiolactone and 1,3-propanesultone. In the reaction, β-propiolactone is converted to carboxybetaine (CB) and 1,3-propanesultone to sulfobetaine (SB). As a result, the produced zwitterionic amphiphiles (named as PMAO-CB-SB) possess CB groups, SB groups, and hydrophobic groups on their backbones. Compared to SB, CB groups are not only zwitterions but also supply carboxyl heads for bioconjugation with conventional EDC/NHS cross-linkers. However, in our experiments we observed that in the bio-crosslinking reaction for only CB-

coated MFNPs, CB can be chemically modified by EDC/NHS, and thus lose its zwitterionic properties and stick to microtube surfaces. In the proposed polymer structure, we used a combination of CB and SB. SB groups are insensitive to regular bio-crosslinking reactions and thus keep the zwitterionic property of the amphiphiles during conjugation. Although simple carboxyl groups are presented on the polymer backbone, CB in the amphiphiles would further increase the biomolecule loading capability of MFNPs through bio-crosslinking. Moreover, CB branches are in the almost same length as SB ones and are easy to access for bioconjugation. In the fabrication of ZW-MFNPs, the PMAO-CB-SB together with hydrophobic MNPs and QDs were dissolved in organic solvents and then dispersed into water under sonication. After dispersion, organic solvents were vacuumed by rotary evaporation. In the dispersion and vacuum, hydrophobic alkyl tails in the amphiphiles interact with hydrophobic MNPs and QDs to form the stable micellar cores, and CB/SB groups are exposed to water. Of note, in our work on ZW-MFNPs, we adopted less toxic I-III-VI chalcopyrite $CuInS_2$/ZnS QDs instead of cadmium-based QDs.[35-41] Moreover, the photoluminescence of $CuInS_2$/ZnS QDs as shown in this work can be tuned from red to near infrared (i.e., 650 nm to 800 nm). They are appropriate for cell/tissue imaging.

In this study, we first synthesized the proposed zwitterionic amphiphiles and characterized them using Fourier transform infrared (FT-IR) spectroscopy and nuclear magnetic resonance (NMR) spectroscopy. Using the developed amphiphiles, we further prepared ZW-MFNPs and characterized these particles in terms of their composition and size, iron content recovery rates, optical properties, colloidal stability, and magnetic relaxivity in harsh conditions using transmission electron microscopy (TEM), energy-dispersive X-ray (EDX) spectroscopy, dynamic light scattering (DLS), UV-Vis spectroscopy, fluorescence spectroscopy, and magnetic

resonance spectroscopy. To explore and demonstrate the potential biomedical applications, we also performed cellular studies to investigate cytotoxicity of ZW-MFNPs and specific cellular binding/uptake of peptide-conjugated ZW-MFNPs by tumor cells.

EXPERIMENTAL METHODS

Materials and Apparatus

Poly(maleic anhydride-*alt*-1-octadecene (PMAO, average M_n 30000-50000), 3-(dimethylamino)-1-propylamine (DMAPA, 99%), N,N-diisopropylethylamine (DIPEA, 99.5%), β-propiolactone (Grade II, ≥90%), gelatin, and poly-D-lysine (PDL) were purchased from Sigma-Aldrich. 1,3-propanesultone (99%) was purchased from Alfa Aesar. Tetrahydrofuran (THF, >99%), ethanol (>99%), methanol (>99%), dichloromethane and chloroform (>99.9%) were purchased from Pharmco-AAPER. U-87 MG (HTB-14) and HEK-293 cells (CRL-1537) were ordered from the American Type Culture Collection (ATCC). RPMI-1640, MEM and DMEM media were from Corning Cellgro. Paraformaldehyde, Dulbecco's phosphate buffered saline (DPBS), and phosphate buffered saline (PBS) were from Fisher Scientific. Heat-inactivated fetal bovine serum (FBS) and stempro accutase were from Gibco. Bovine serum albumin (BSA) was from MP Biomedicals. Chlorotoxin (CTX) was purchased from Alomone Labs. Fluorescein diacetate (FDA), propidium iodide (PI), 4',6-diamidino-2-phenylindole (DAPI) were was from Pierce. All chemicals or reagents were used as received without further purification. $CuInS_2/ZnS$ QDs and $MnFe_2O_4$ magnetic nanoparticles were prepared and characterized by the authors following their previous work.[20, 41]

The infrared (IR) spectra were acquired using a Perkin-Elmer Frontier FT-IR spectrometer equipped with Spectrum 10 software and Universal ATR sampling accessory. The nuclear

magnetic resonance (NMR) spectra were obtained on Varian VNMRS operating at 500MHz (^{1}H) and 298K. For the ZW-MFNP preparation, a probe-type Misonix Ultrasonic Liquid Processor (QSonica) was used. Transmission electron microscope (TEM) images and Energy-dispersive X-ray (EDX) spectra were acquired using a JEOL analytical transmission electron microscope (model JEM 2100F) operated with a 200 kV acceleration voltage and equipped with an Oxford Energy-Dispersive X-ray (EDX) spectrometer. The optical characteristics of ZW-MFNPs including ultraviolet-visible (UV-Vis) and photoluminescence spectra were collected using Shimadzu UV-2450 spectrometer and Shimadzu RF-5301PC spectrofluorometer. The hydrodynamic sizes were measured in H_2O using a Malvern Zetasizer Nano ZS dynamic light scattering (DLS) instrument equipped with a HeNe laser operating at 632.8 nm and a scattering detector at 173 degrees. For iron content assay and colloidal stability study, a Perkin-Elmer microplate reader was used. Cell viability or cytotoxicity were estimated using a BD Biosciences SORP LSR II flow cytometer with 4 lasers (405 nm, 488 nm, 561 nm and 640 nm) and 18 fluorescence detectors. Magnetic resonance imaging was performed on a Bruker BioSpec 7T horizontal bore system. Fluorescent cellular images were taken using Leica TCS SP8 (DM 6000 CS) confocal scanning microscope.

Preparation of Zwitterionic Amphiphiles

PMAO-DMAPA was first prepared by stirring the mixture of 2.02 g PMAO and 1.1 mL DMAPA in 25 mL CH_2Cl_2 over ice-bath for 3h followed by precipitation of the product by adding acetone. The white precipitate was collected by filtration and then washed 3 times (with sonication) by dissolving in ~15-20 mL $CHCl_3$ and precipitating with acetone (3 times volume excess). The product was dried under vacuum overnight resulting in 2.03g (~77% yield) of

PMAO-DMAPA. For the synthesis of PMAO-DMAPA-CBSB, the mixture of 0.50 g PMAO-DMAPA, 192 μL DIPEA, 38.4 μL of β-propiolactone, and 68.2 mg 1,3-propanesultone in 5 mL CH_2Cl_2 was stirred over ice-bath for ~3 hours and then at room temperature overnight. The resulting lightly cloudy mixture was pipetted into centrifuge tubes and washed (> 5 times) by dissolving in ~1 mL $CHCl_3$-MeOH (1:1, v/v), precipitating with acetone (3-5 times volume) and collecting the precipitate by centrifugation. The white solid was dried under vacuum overnight giving 0.54 g of product (~88% yield).

Preparation of ZW-MFNPs

The solution of 0.6 mg $MnFe_2O_4$ MNPs and 2.4 mg $CuInS_2$/ZnS QDs in THF (900 μL) and 1.7 mg PMAO-CBSB in $CHCl_3$-MeOH (~ 50 μL) was layered on top of cold water in a glass vial. The mixture was ultrasonicated using the Misonix Ultrasonic Liquid Processor with a 5 W output power for 1 min. After sonication, the organic solvents were removed by rotary evaporation at room temperature and the sample filtered through a 0.2 μm syringe filter. Empty micelles or single-nanoparticle based micelles were removed by centrifugation at 18,000 rpm for 25 min (twice). The collected ZW-MFNPs were dispersed in 400 μL of water, and stored at 4°C until further use.

Cell Cytotoxicity of MFNPs

A U-87 MG human brain glioblastoma cell line was cultured (37 °C, 5% CO_2) on 24-well plastic plates in MEM medium with 10% FBS overnight. The human embryonic kidney cell line HEK-293 was cultured (37 °C, 5% CO_2) on 24-well plastic plates in RPMI-1640 medium with 10% FBS overnight. For the ZW-MFNP cytotoxicity study, cells were incubated with ZW-

MFNPs in growth medium at various concentrations. After 24-hr incubation, cells were gently rinsed with DPBS and released from well bottom using stempro accutase, and then stained with FDA and PI to determine live versus dead cells. Dead cells (red staining by PI) and live cells (green staining by FDA) were counted using a BDBiosciences SORP LSR II flow cytometer. The cell viability was calculated as the ratio of live cells over the sum of live cells and dead cells.

Tumor Cell Targeting Using Peptide Conjugated ZW-MFNPs

ZW-MFNPs were conjugated with CTX via EDC/sulfo-NHS mediated reaction. Briefly, 60 μL of the collected ZW-MFNPs were reacted with 50 μg CTX with the assistance of EDC/sulfo-NHS in PBS for 2 ~ 3 hours. The CTX-conjugated ZW-MFNPs were washed using centrifuge, suspended in 250 μL PBS, and stored at 4°C before use. A U-87 MG human brain glioblastoma cell line was cultured (37 °C, 5% CO_2) on glass coverslip coated with gelatin in MEM medium with 10% FBS until 50 - 80% confluency was achieved. The human embryonic kidney cell line HEK-293 was cultured (37 °C, 5% CO_2) on glass coverslip coated with PDL (poly-D-lysine) in RPMI-1640 medium with 10% FBS until 50 - 80% confluency was achieved. For the ZW-MFNP tumor cell targeting study, cells were incubated with CTX conjugated ZW-MFNP in DMEM with 2% BSA at various concentrations. As control, cells were also incubated with non-conjugated ZW-MFNPs. After 2-hr incubation, cells were gently rinsed three times with PBS, fixed with 4% PFA in PBS solution for 20 minutes and washed three times with PBS. For cellular nuclei staining, cells were incubated with DAPI, washed three times with PBS, and then mounted on glass slides. Cells were imaged using a Leica confocal microscope and images were analyzed using ImageJ. The statistical significance ($p < 0.05$) was determined by the single-tailed student t test.

RESULTS AND DISCUSSION

The synthesis of zwitterionic amphiphilic polymer PMAO-CB-SB involved two steps. In the first step, PMAO anhydride rings were opened by the primary amine groups of DMAPA. The ring opening resulted in the presence of terminal carboxyl and tertiary amine groups on the polymer backbone. In the second step, tertiary amines reacted with β-propiolactone and 1,3-propanesultone to form CB and SB groups, respectively. To avoid possible ring-opening polymerization of β-propiolactone and/or 1,3-propanesultone,[42] the second-step reaction was started in ice-bath and the total molarity of both β-propiolactone and 1,3-propanesultone was controlled to be slightly higher than that of tertiary amines (if all anhydride rings in PMAO were opened). In this study a 1:1 ratio of them was used to demonstrate the proof of concept on PMAO-CB-SB. The synthesis is simple, and its production yield is > 80%. The synthesized PMAO derivatives were characterized by FTIR, as shown in Figure 2. PMAO-DMAPA spectrum showed the disappearance of anhydride C=O at around 1857 cm^{-1} and 1776 cm^{-1}, and the appearance of new peaks at around 1713 cm^{-1} for carboxyl C=O, around 1649 cm^{-1} for amide C=O, and around 1560 cm^{-1} for amide N-H. These spectral changes indicate the addition of DMAPA to PMAO. In the spectrum of PMAO-CB-SB, the peaks from PMAO-DMAPA are represented and some new peaks at around 1175 cm^{-1} and 1035 cm^{-1} are observed. As shown in Figure S1, the peaks at around 1175 cm^{-1} and 1035 cm^{-1} are also observed in the FTIR spectrum of amidosulfobetaine-16 (ASB-16) which is an alkyl chain with a SB head. These two peaks represent S=O in the sulfo group. The spectrum comparison and analysis indicates the formation of SB after the reaction of the tertiary amines of PMAO-DMAPA with 1,3-propanesultone.[43-46] Peaks associated with CB in PMAO-CB-SB are not significant for observation, probably because the peaks for the additional carboxyl C=O from the formed CB groups in PMAO-CB-SB are

overlapping with those of the existing carboxyl C=O in PMAO-DMAPA. However, a slight distortion at around 1590 cm^{-1} in the spectrum of PMAO-CB-SB (not marked but close to the mark line at 1560 cm^{-1}) is still distinguishable. Because a significant peak at around 1590 cm^{-1} for N-Dodecyl-N,N-(dimethylammonio)butyrate (DDMAB), an alkyl chain with a CB head, is observed (as shown in Figure S1), this minor distortion at around 1590 cm^{-1} in the spectrum of PMAO-CB-SB may suggest the addition of CB to PMAO.

The synthesized PMAO derivatives dissolved in a mixture of $CDCl_3$ and CD_3OD were further characterized using NMR. All NMR spectra were presented in Figure S2. For all samples, the hydrophobic alkyl chain (C_{18}) of the polymer was observed at 0.80 ppm for $–CH_3$ and 1.18 ppm for $–CH_2$. For PMAO-DMAPA, two additional peaks are presented at 2.66 ppm and 1.76 ppm. In the literature, the following peaks have been reported for the attachment of DMAPA to polymer backbones: C(O)NHCH_2 at 3.2-3.3 ppm, $CH_2N(CH_3)_2$ at 2.36 ppm, $N(CH_3)_2$) at 2.2 ppm, $CH_2CH_2N(CH_3)_2$ at 1.6 ppm.[47-49] The observed peaks due to the addition of DMAPA to PMAO appear in the chemical shift range as reported in the literature for the same chemical group. For PMAO-CB-SB, it has two peaks at 1.88 ppm and 2.75 ppm (similar to those of PMAO-DMAPA), but have an additional peak at around 3.02 ppm. Literature has reported the following peaks due to the CB addition to polymer backbones: C(O)NHCH_2 at 2.75-3.48 ppm, $C(O)NHCH_2CH_2$ at 1.55-2 ppm, $CH_2N^+(CH_3)_2$ at 2.75-3.48 ppm, $N^+(CH_3)_2$ at 2.9-3.3 ppm, $CH_2CH_2COO^-$ at 3.4-3.55 ppm, CH_2COO^- at 2.25-2.75 ppm; and the follow peaks due to the SB addition to polymer backbones: C(O)NHCH_2 at 3.2 ppm, $C(O)NHCH_2CH_2$ at 1.9 ppm, $CH_2N^+(CH_3)_2$ at 3.3 ppm, $N^+(CH_3)_2$ at 3.05-3.1 ppm, $CH_2CH_2CH_2SO_3^-$ at 3.4 ppm, $CH_2CH_2SO_3^-$ at 2.15 ppm, and $CH_2CH_2SO_3^-$ at 2.89 ppm.[50-55] The peaks for PMAO-CB-SB match with what were reported.

Of note, in the preparation of zwitterionic amphiphilic polymers, although the molar ratio between β-propiolactone and 1,3-propanesultone can be tuned to adjust the ratio of CB and SB on the polymer backbone, it is good to keep a certain amount of CB groups on polymers for the cross-linking with other molecules. To maximally demonstrate the effect of CB groups on facilitating the cross-linking, PMAO-CB (100% CB and 0% SB) and PMAO-SB (0% CB and 100% SB) were prepared and they were further conjugated with amino fluorophores (amino Cy3 from Lumiprobe, Inc.) in organic phase through EDC cross-linking. In the conjugation process, the same mole (2 μmole) of PMAO-CB and PMAO-SB were reacted with a mixture of 0.4 nmole amino Cy3 and 1.2 nmole EDC, respectively. PMAO-CB conjugates (after wash using 48-hr dialysis) present a higher fluorescence intensity of Cy3 compared to PMAO-SB conjugates (data shown in Figure S3). We attribute this higher intensity to more accessible carboxyl groups in PMAO-CB for cross-linking.

On the basis of the synthesized PMAO-CB-SB, ZW-MFNPs integrating small $MnFe_2O_4$ MNPs and $CuInS_2$/ZnS QDs in the micellar cores were fabricated. MNPs and QDs are around 5 nm. In our approach in preparing $CuInS_2$ QDs, the QD photoluminescence can be tuned from 650 nm ~ 800 nm (refer to Figure S4). In this work, we prepared $CuInS_2$ QDs with around 720 nm photoluminescence emission, and after ZnS shell growth the $CuInS_2$/ZnS QDs emit photoluminescence at around 685 nm. The fabricated ZW-MFNPs were characterized using TEM and EDXS. Figure 3 (a) and (b) present TEM images of ZW-MFNPs, which indicate the sizes of most of ZW-MFNPs in around 50 ~ 60 nm. On the basis of TEM imaging, the overall size of ZW-MFNPs mostly distributed over a range of 20 ~ 150 nm was observed. EDX analysis in Figure 3(c) further demonstrates that ZW-MFNPs are composed of Mn, Fe, O, Cu, In, Zn and S elements. Figure S5 shows the TEM image of blank particles formed by only using

PMAO-CB-SB polymers (without loading any QDs and MNPs). To acquire the TEM image of the blank particles, 1% phosphotungstic acid was used to negatively stain the blank particles. The sizes of the blank particles are relatively smaller compared to ZW-MFNPs. It is reasonable because the core of particles is empty without loading extra materials (QDs, MNPs) to increase its size. In addition to TEM, DLS data of ZW-MFNPs have been collected and presented in Table 1. The hydrodynamic sizes of ZW-MFNPs are 99 nm with a standard deviation at 60 nm. The ZW-MFNP hydrodynamic sizes mainly are contributed by the micelle hydrophobic core (imaged by TEM), the polymer shell, and the hydration layer caused by zwitterions on the polymer shell.

The (Mn + Fe) content in ZW-MFNPs was also quantified on the basis of the iron content determination of ZW-MFNPs using thiocyanate colorimetry. In this colorimetry, ZW-MFNPs were first dissolved in H_2SO_4. Potassium permanganate ($KMnO_4$) was then added dropwise into the dissolved sample until the purple color was retained. Afterwards, the purple sample and KSCN were mixed, and the resultant red solution was loaded into a microplate and the absorbance of the resultant solution was measured at 490 nm using the microplate reader. Solutions of $FeCl_3$ in H_2SO_4 with a wide iron(III) concentration range were used as calibration standards. Iron content of ZW-MFNPs was determined by interpolating the absorbance of the samples on the calibration curve. Iron content in the starting magnetic materials ($MnFe_2O_4$ magnetic nanoparticles) used for the ZW-MFNP preparation was also determined in the same way. After iron determination, (Mn + Fe) content in ZW-MFNPs was further determined on the basis of the atomic ratio of Mn:Fe in $MnFe_2O_4$ magnetic nanoparticles. The (Mn+Fe) recovery rate was calculated as the mass ratio of the measured (Mn+Fe) in ZW-MFNPs and the measured (Mn+Fe) in the starting magnetic materials used for ZW-MFNP preparation. A detailed

experiment steps for this colorimetry can be found in our previous work.[20] In this study, the (Mn + Fe) recovery rate for 0.6 mg MNPs input to ZW-MFNPs is as high as around 60%, as shown in Table 1.

The photoluminescence spectrum of ZW-MFNPs is shown in Figure 4(a), compared to that of QDs in organic solvents. The photoluminescence intensities are scaled by the quantum yield of ZW-MFNPs relative to that of hydrophobic QDs in THF (the measured quantum yields of ZW-MFNPs are < 10 %). It can be seen that the photoluminescence of ZW-MFNPs is significantly quenched. The quenching may be caused by the MNP absorption on QD emissions, or by the reduction of QD excitation/emission surfaces due to the blocking effect of surrounding MNPs. It should be noted that ZW-MFNPs with low quantum yields are adequate for optical imaging applications.[56]

The magnetic imaging features of MFNPs were characterized using a magnetic resonance imaging (MRI) instrument (Bruker BioSpec). The MR images of ZW-MFNPs were acquired with a conventional spin echo acquisition (TR = 6000 ms) with TE values ranging from 9.5 ms to 190 ms. T_2 parameter (or R_2 parameter, $R_2=1/T_2$) of ZW-MFNPs was extracted by fitting the exponential decay of the signal waveform and measuring the signal intensity at a series of different TE values. Figure 4(b) presents R_2 parameter (or $1/T_2$) of ZW-MFNPs vs (Mn + Fe) concentration. The relaxivity (r_2) of ZW-MFNPs was calculated as the slope of the R_2 curve. The relaxivity r_2 value of ZW-MFNPs is around 150 $mM^{-1}s^{-1}$. R_2 parameter of ZW-MNPs (using MNPs and the synthesized zwitterionic amphiphiles but not containing any QDs) also was measured for comparison. The relaxivity r_2 of ZW-MNPs is around 266 $mM^{-1}s^{-1}$. In literature, T_2 parameter of agglomerated nanomagnet clusters has been formulated and discussed.[57] Briefly, for agglomerated nanomagnets, $1/T_2=16f_a\Delta\omega^2\tau_D/45$ with f_a being the volumic fraction occupied

by the agglomerated nanomagnets, $\Delta\omega = \mu_o M\gamma/3$ (where μ_o is the vacuum magnetic permeability, M is the particle magnetization, and γ is the proton gyromagnetic ratio), and τ_D is the translational diffusion time around the cluster ($\tau_D = R_a^2/D$ where R_a being the cluster radius and D being the water diffusion coefficient). Although the formula of T_2 parameter discussed for the agglomerated system is built only on small magnetic nanoparticles, it can be applicable to ZW-MFNPs with a mixture of QDs and MNPs. Specifically, f_a probably can be re-defined as the volumic fraction occupied by MNPs in ZW-MFNPs. Considering ZW-MFNPs and ZW-MNPs have the similar size ranges (as shown in Table 1), the increase of QDs over MNPs in the fabrication may cause the decrease of f_a, which further result in the total net magnetization (M) of ZW-MFNPs to drop. Thus, QDs involved in the fabrication cause R_2 and thus r_2 decrement of ZW-MFNPs. In spite of the R_2 or r_2 drop, the relaxivity value for ZW-MFNPs is still comparable to many reported ones.[58-59] Please be noted that the fabricated ZW-MNPs also can be considered as excellent contrasts for MRI because of their high magnetic relaxivity and (Mn + Fe) recovery rate.

In biosensing/imaging applications, aggregation of ZW-MFNPs will cause the degradation or even loss of their physiochemical and biological functionalities. Thus ZW-MFNPs are expected to have excellent colloidal stability. The photoluminescence intensity of ZW-MFNPs dispersed in PBS-5%FBS with pH 4-9, a 1 M NaCl-5%FBS and human serum was monitored over 72 hours at 37 °C using a microplate reader, and presented in Figure 5. The photoluminescence intensity and hence stability of these ZW-MFNPs was maintained in all these conditions. Moreover, no precipitates or significant photoluminescence intensity decreases were observed over one week at 37 °C. Stored at 4 °C, the ZW-MFNPs were also found to be stable in water at over at months (Figure S6). The excellent stability of these ZW-MFNPs in these conditions

especially in a solution with pH4, a solution with 1M salinity, and serum, is very attractive. CB groups and SB groups coated on the surface of ZW-MFNPs should be attributed to this stability. These zwitterions facilitate a hydration layer coating on ZW-MFNPs. The hydration layer is very stable and almost remains unperturbed under harsh conditions such as high/low pHs, high salinity, and complex matrix. The stability of ZW-MFNPs offers a great deal of flexibility for their biomedical applications.

The cytotoxicity of the ZW-MFNPs was studied using human primary glioblastoma cells (U-87 MG) and human embryonic kidney 293 cells (HEK-293). U-87 MG and HEK-293 represent tumor cells and normal cells, respectively. Figure 6 shows the measured cell viabilities for U-87 MG and HEK-293 after 24-hour incubation with ZW-MFNPs under different concentrations, respectively. It can be seen that the cell viabilities under different particle concentrations are comparable to controls, and thus the ZW-MFNPs are biocompatible and their cytotoxicity is minimal.

For cellular imaging studies, we adopted CTX as a targeting ligand. CTX is a 36-amino acid peptide that specifically binds to matrix metalloproteinase II (MMP-2) present on the surface of glioma cells with high affinity.[60-61] The specific binding results in loss of gelatinase activity, disruption in chloride channel currents, reduction in both MMP-2 and chloride channel expressions, and internalization of chloride channels. U-87 is a human primary glioblastoma cell line expressing MMP-2 receptors, and CTX can specifically bind to and be internalized into U-87. To investigate whether CTX-conjugated ZW-MFNPs can be specifically targeted to and internalized into U-87, we used a nonmalignant cell line human embryonic kidney 293 (HEK-293) as a control. Figure 7 (a-d) present the representative overlaid confocal images demonstrating the cellular uptake/internalization when each type of cells were incubated with

CTX-conjugated and non-conjugated ZW-MFNPs under the same concentration of particles (i.e., 0.1 μg (Mn+Fe)/mL). Corresponding to each overlaid image in Figure 7 (a-d), Figure S7 shows the associated confocal images at different channels. Figure 7(e) shows the fluorescence intensity per unit cytoplasm area (counting > 200 cells) under a series of ZW-MFNP concentrations. It can be seen that U-87 cells do internalize more CTX-conjugated ZW-MFNPs than HEK-293, and non-conjugated ZW-MFNPs present no significant cellular uptake by both cell lines. Through this comparison, it can be concluded that CTX-conjugated ZW-MFNPs are specific to U-87. It was also observed that HEK-293 did internalize some CTX-conjugated ZW-MFNPs at high concentrations. It is believed that the cellular uptake of CTX-conjugated micelles may involve pinocytosis mechanisms in high concentration ranges.[62-63]

CONCLUSION

In summary, starting with PMAO polymers, we applied appropriate approaches to open and convert anhydride rings in the polymers to the desired zwitterionic groups, and thus modified PMAO polymers to zwitterionic amphiphiles. Utilizing the zwitterionic amphiphiles together with $MnFe_2O_4$ MNPs and $CuInS_2$/ZnS QDs, ZW-MFNPs were further fabricated through a simple and fast self-assembling process. The produced ZW-MFNPs possess several merits including dual imaging properties, high (Mn + Fe) recovery, excellent stability in aqueous solutions with a wide pH/ionic-strength range and physiological media, minimal cytotoxicity, and brain tumor cell targeting after bioconjugation with CTX. It is believed that the high (Mn + Fe) recovery of ZW-MFNPs is attributed to the efficient wrapping of MNPs by long backbone and multiple alkyl tails of the synthesized amphiphiles, and the colloidal stability and the minimal cytotoxicity for tumor cell targeting are resulted from the nature of the incorporated

zwitterionic groups. The cellular imaging studies, together with the photoluminescence tunability of $CuInS_2$/ZnS QDs from the visible to near infrared (NIR) range, suggest that ZW-MFNPs can be applied for *in vivo* diagnosis.[64] The MR and NIR fluorescence imaging data obtained from the same ZW-MFNP probes may provide complimentary information on tumor biology and thus enhance diagnosis accuracy. Notably, although the developed zwitterionic amphiphile was applied for ZW-MFNPs in this work, it is also valuable for the surface modification of many other hydrophobic nanoparticles.

ACKNOWLEDGEMENT

This research was supported by the National Institute of Health (NIH) through the grant #1P20GM103650.

REFERENCES

1. W. H. Suh, Y. H. Suh and G. D. Stucky, Nano Today, 2009, **4**, 27–36.
2. S. A. Corr, Y. P. R. Akovich and Y. K. Gun'ko, Nanoscale Res. Lett., 2008, **3**, 87-104.
3. S. T. Selvan, Biointerphases, 2010, 5, Fa110–Fa115.
4. K. D. Mahajan, Q. Fan, J. Dorcéna, G. Ruan and J. O. Winter, Biotech. J., 2013, **8**, 1424-1434.
5. H. W. Gu, R. K. Zheng, X. X. Zhang and B. Xu, J. Am. Chem. Soc., 2004, **126**, 5664–5665.
6. C. Y. Ang, L. Giam, Z. M. Chan, A. W. H. Lin, H. Gu, E. Devlin, G. C. Papaefthymiou, S. T. Selvan and J. Y. Ying, Adv. Mater., 2009, **21**, 869-873.
7. N. Singh, S. Charan, K. Sanjiv, S. H. Huang, Y. C. Hsiao, C. W. Kuo, F. C. Chien, T. C. Lee and P. Chen, Bioconjugate Chem., 2012, **23**, 421-430.

8. M. Singh, T. Atkins, E. Muthuswamy, S. Kamali, C. Tu, A. Y. Louie and S. M. Kauzlarich, ACS Nano, 2012, **6**, 5596-5604.
9. O. Chen, L. Riedemann, F. Etoc, H. Herrmann, M. Coppey, M. Barch, C. T. Farrar, J. Zhao, O. T. Bruns, H. Wei, P. Guo, J. Cui, R. Jensen, Y. Chen, D. K. Harris, J. M. Cordero, Z. Wang, A. Jasanoff, D. Fukumura, R. Reimer, M. Dahan, R. K. Jain and M. G. Bawendi, Nat. Commun., 2014, **5**, doi:10.1038/ncomms6093.
10. D. K. Yi, S. T. Selvan, S. S. Lee, G. C. Papaefthymiou, D. Kundaliya and J. Y. Ying, J. Am. Chem. Soc., 2005, **127**, 4990–4991.
11. J. Kim , J. E. Lee , J. Lee , J. H. Yu , B. C. Kim, K. An , Y. Hwang , C. Shin , J. Park , J. Kim and T. Hyeon, J. Am. Chem. Soc., 2006, **128**, 688–689.
12. J. Kim, H. S. Kim, N. Lee, T. Kim, H. Kim, T. Yu, I. C. Song, W. K. Moon and T. Hyeon, Angew. Chem. Int. Ed., 2008, **47**, 8438–8441.
13. S. T. Selvan, P. K. Patra, C. Y. Ang and J. Y. Ying, Angew. Chem. Int. Ed., 2007, **119**, 2500-2504.
14. D. Wang, J. He, N. Rosenzweig and Z. Rosenweig, Nano. Lett., 2004, **4**, 409-413.
15. R. Di Corato, N. C. Bigall, A. Ragusa, D. Dorfs, A. Genovese, R. Marotta, L. Manna and T. Pellegrino, ACS Nano, 2011, **5**, 1109-1121.
16. B. S. Kim and T. A. Taton, Langmuir, 2007, **23**, 2198-2202.
17. J. H. Park, G. von Maltzahn, E. Ruoslahti, S. N. Bhatia and M. J. Sailor, Angew. Chem. Int. Ed., 2008, **120**, 7394-7398.
18. E. F. Erogbogbo, K. T. Yong, R. Hu, W. C. Law, H. Ding, C. W. Chang, P. N. Prasad and M. T. Swihart, ACS Nano, 2010, **4**, 5131-5138.

19. H. M. Kim, H. Lee, K. S. Hong, M. Y. Cho, M. H. Sung, H. Poo and Y. T. Lim, ACS Nano, 2011, **5**, 8230-8240.
20. V. G. Demillo, M. Liao, X. Zhu, D. Redelman, N. G. Publicover and K. W. Hunter Jr, Colloids Surf., A, 2014, **464**, 134-142.
21. W. Yu, E. Chang, J. Falkner, J. Zhang, A. Al-Somali, C. Sayes, J. Johns, R. Drezek and V. Colvin, J. Am. Chem. Soc., 2007, **129**, 2871–2879.
22. C. Fang, N. Bhattarai, C. Sun and M. Zhang, Small, 2009, **5**, 1637-1641.
23. E. Muro, T. Pons, N. Lequeux, A. Fragola, N. Sanson, Z. Lenkei and B. Dubertret, J. Am. Chem. Soc., 2010, **132**, 4556-4557.
24. B. Yameen, W. Choi, C. Vilos, A. Swami, J. Shi and O. C. Farokhzad, J. Control. Release, 2014, **190**, 485-499.
25. W. Yang, S. Liu, T. Bai, A. J. Keefe, L. Zhang, J. Ella-Menye, Y. Li and S. Jiang, Nano Today, 2014, **9**, 10-16.
26. T. Ishida and H. Kiwada, Int. J. Pharm., 2008, **354**, 56–62.
27. K. Knop, R. Hoogenboom, D. Fischer and U. S. Schubert, Angew. Chem. Int. Ed., 2010, **49**, 6288–6308.
28. E. Muro, A. Fragola, T. Pons, N. Lequeux, A. Ioannou, P. Skourides and B. Dubertret, Small, 2012, **8**, 1029-1037.
29. H. T. Uyeda, I. L. Medintz, J. K. Jaiswal, S. M. Simon and H. Mattoussi, J. Am. Chem. Soc., 2005, **127**, 3870-3878.
30. K. Susumu, E. Oh, J. B. Delehanty, J. B. Blanco-Canosa, B. J. Johnson, V. Jain, W. J. Hervey, IV, W. R. Algar, K. Boeneman, P. Dawson and I. Medintz, J. Am. Chem. Soc., 2011, **133**, 9480-9496.

31. J. Park, J. Nam, N. Won, H. Jin, S. Jung, S. Jung, S. Cho and S. Kim, Adv. Funct. Mater., 2011, **21**, 1558-1566.

32. V. V. Breus, C. D. Heyes, K. Tron and G. U. Nienhaus, ACS Nano, 2009, **3**, 2573–2580.

33. H. Wei, N. Insin, J. Lee, H. Han, J. Cordero, W. Liu and M. Bawendi, Nano Lett., 2012, **12**, 22-25.

34. X. Liu, H. Huang, G. Liu, W. Zhou, Y. Chen, Q. Jin and J. Ji, Nanoscale, 2013, **5**, 3982-3991.

35. L. Li, T. Daou, I. Texier, T. Chi, N. Liem and P. Reiss, Chem. Mater., 2009, **21**, 2422-2429.

36. L. Li, A. Pandey, D. J. Werder, B. P. Khanal, J. M. Pietryga and V. I. Klimov, J. Am. Chem. Soc., 2011, **133**, 1176–1179.

37. J. Park, C. Dvoracek, K. H. Lee, J. F. Galloway, H. C. Bhang, M. G. Pomper and P. C. Searson, Small, 2011, **7**, 3148-3152.

38. H. Zhong, Z. Bai and B. Zou, J. Phys. Chem. Lett., 2012, **3**, 3167-3175.

39. D. Deng, Y. Chen, J. Cao, J. Tian, Z. Qian, S. Achilefu and Y. Gu, Chem. Mater., 2012, **24**, 3029-3037.

40. L. Huang, X. Zhu, N. G. Publicover, K. W. Hunter, M. Ahmadiantehrani, A. de Bettencourt-Dias and T. W. Bell, J. Nanopart. Res., 2013, **15**, doi: 10.1007/s11051-013-2056-9.

41. R. Shrake, V. G. Demillo, M. Ahmadiantehrani, X. Zhu, N. G. Publicover and K. W. Hunter Jr., J. Colloid Interface Sci., 2014, **437**, 140-146.

42. T. L. Gresham , J. E. Jansen and F. W. Shaver, J. Am. Chem. Soc., 1948, **70**, 998–999.

43. G. Karakus, Z. A. Polat, A. F. Yenidunya, H. B. Zengin and C. B. Karakus, Polym. Int., 2013, **62**, 492-495.

44. E. Peng, E. Shi, G. Choo, Y. Sheng and J. M. Xue, New Journal of Chemistry, 2013, **37**, 2051-2060.

45. J. Sun, Z. Yu, C. Hong and C. Pan, Macromol. Rapid Commun., 2012, **33**, 811−818.

46. J. Yuan, S. Lin and J. Shen, Colloids Surf. B, 2008, **66**, 90-95.

47. L. Wu, J. Jasinski and S. Krishnan, J. Appl. Polym. Sci., 2012, **124**, 2154-2170.

48. Z. Chu and Y. Feng, Synlett, 2009, 2655-2658.

49. H. Tan and H. Xiao, Tetrahedron Lett., 2008, **49**, 1759-1761.

50. N. D. Brault , A. D. White , A. D. Taylor , Q. Yu and S. Jiang, Anal. Chem., 2013, **85**, 1447-1453.

51. N. Y Kostina, S. Sharifi, A. de los Santos Pereira, J. Michálek, D. W. Grijpma and C. Rodriguez-Emmenegge, J. Mater. Chem. B, 2013, **1**, 5644-5650.

52. L. Wang, Z. Wang, G. Ma, W. Lin and S. Chen, Langmuir, 2013, **29**, 8914-8921.

53. U. Edlund, C. Rodriguez-Emmenegger, E. Brynda and A. Albersson, Polym. Chem., 2012, **3**, 2920-2927.

54. C. Rodriguez-Emmenegger, B. Schmidt, Z. Sedlakova, V. Šubr, A. B. Alles, E. Brynda and C. Barner-Kowollik, Macromol. Rapid Commun., 2011, **32**, 958-965.

55. M. G. D'Andrea, C. C. Domingues, S. V. P. Malheiros, F. G. Neto, L. R. S. Barbosa, R. Itri, F. C. L. Almeida, E. Paula and M. L. Bianconi, Langmuir, 2011, **27**, 8248-8256.

56. J. Zimmer, S. Kim, S. Ohnishi, E. Tanaka, J. Frangioni and M. Bawendi, J. Am. Chem. Soc., 2006, 128, 2526-2527.

57. S. Laurent, D. Forge, M Port, A. Roch, C. Robic, L. V. Elst and R. N. Muller, Chem. Rev., 2008, **108**, 2064–2110.

58. H. B. Na, I. C. Song and T. Hyeon, Adv. Mater., 2009, **21**, 2133-2148

59. C. Xu and S. Sun, Adv. Drug Deliv. Rev., 2013, **65**, 732-743

60. P. M. Costa, A. L. Cardoso, L. S. Mendonça, A. Serani, C. Custódia, M. Conceição, S. Simões, J. N. Moreira, L. Pereira de Almeida and M. C. Pedroso de Lima, Mol. Ther. Nucleic Acids, 2013, **2**, e100.

61. O. Veiseh, C. Sun, C. Fang, N. Bhattarai, J. Gunn, F. Kievit, K. Du, B. Pullar, D. Lee, R. G. Ellenbogen, J. Olson and M. Zhang, Cancer Res., 2009, **69**, 6200–6207.

62. J. L. Kovar, E. Curtis, S. F. Othman, M. A. Simpson and D. M. Olive, 2013 Anal. Biochem., 2013, **440**, 212-219.

63. E. M. Burns, G. D. Dobben, T. W. Krukeberg and P. K. Gaetano, Adv. Neurol., 1981, **30**, 159-165.

64. H. Liao, Z. Wang, S. Chen, H. Wu, X. Ma and M. Tan, RSC Adv., 2015, **5**, 66575-66581.

FIGURES, TABLES AND CAPTIONS

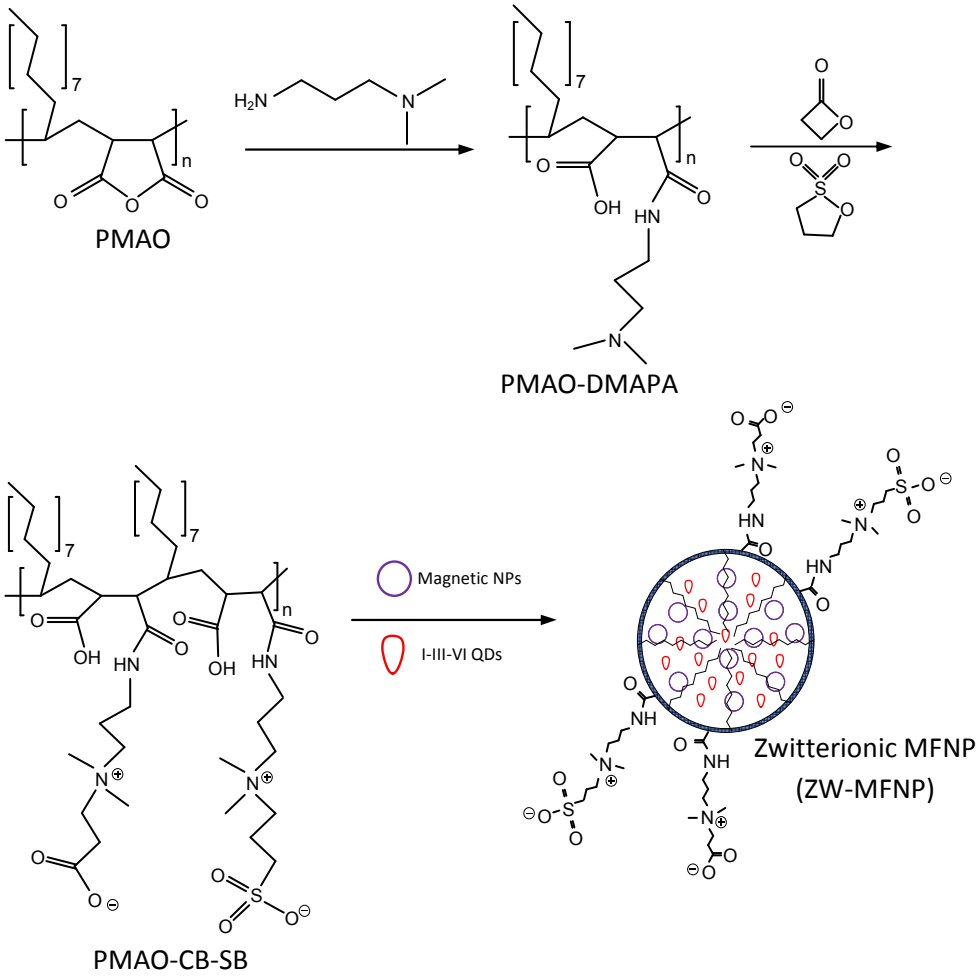

Figure 1. Scheme of the preparation process for zwitterionic magnetofluorescent nanoparticles (ZW-MFNPs) – anhydride rings in PMAO are opened by DMAPA, the produced terminal tertiary amines in PMAO-DMAPA react with β-propiolactone and 1,3-propanesultone to form terminal carboxybetaine (CB) and sulfobetaine (SB), and the produced zwitterionic amphiphiles PMAO-CB-SB are used to encapsulate both MNPs and QDs through self-assembly.

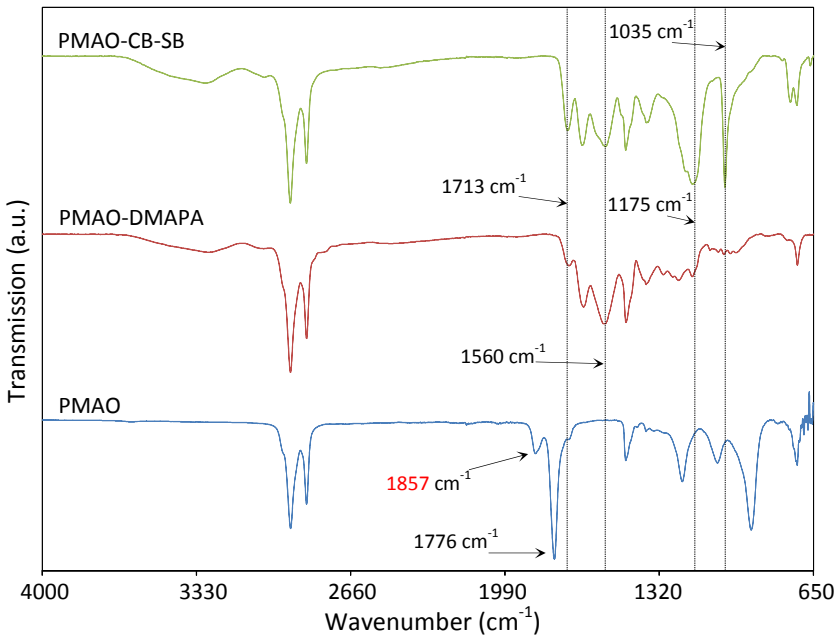

Figure 2. FT-IR spectra of PMAO derivatives in the synthesis of PMAO-CB-SB

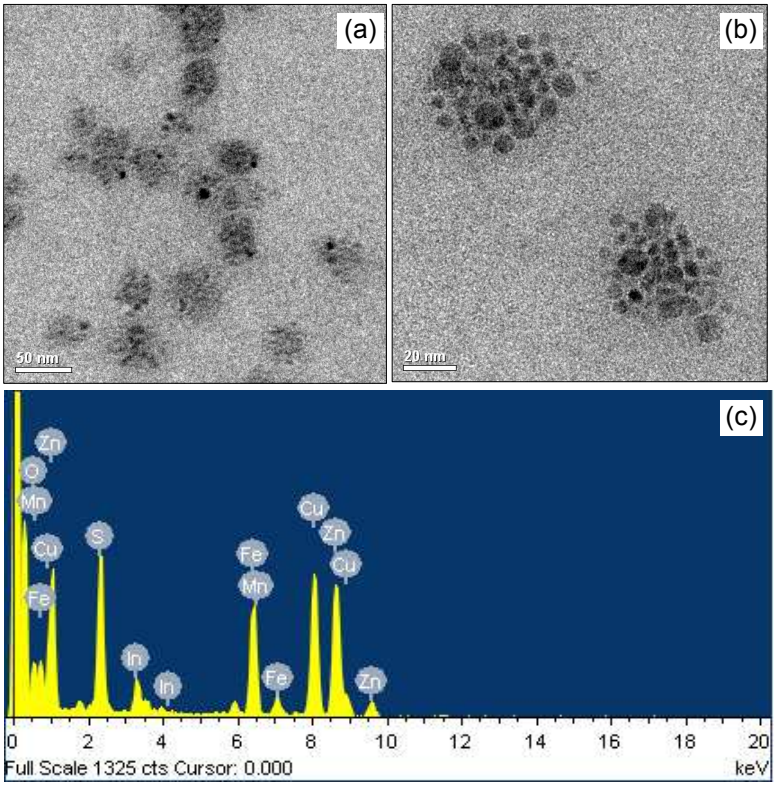

Figure 3. (a) and (b) Representative TEM images of ZW-MFNPs; (c) EDX spectrum of ZW-MFNPs illustrating Mn, Fe, O, Cu, In, Zn and S elements which are composites of MNPs and QDs.

Table 1. Hydrodynamic sizes and (Mn+Fe) recovery rates of ZW-MFNPs and ZW-MNPs

Particles	Hydrodynamic sizes (nm)	(Mn + Fe) recovery rates (%)
ZW-MFNPs	99 ± 60	62 ± 1
ZW-MNPs	133 ± 69	60 ± 4

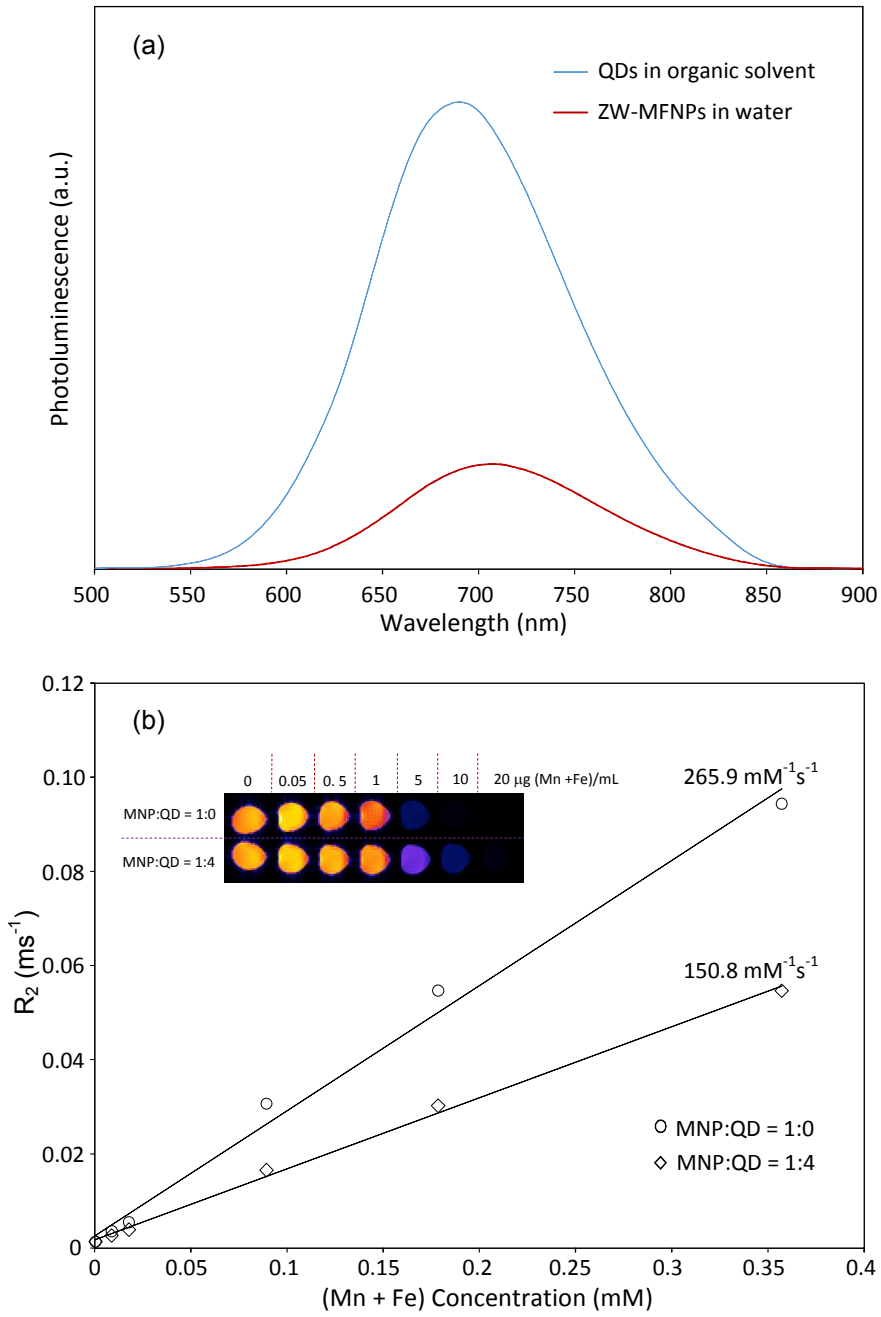

Figure 4. (a) Photoluminescence spectra of hydrophobic QDs in organic solvent and water-soluble ZW-MFNPs; (b) R_2 parameters of ZW-MFNPs vs (Mn + Fe) concentration (the slope r_2 of each curve = R_2/[(Mn + Fe) concentration]). The inset image is a representative magnetic resonance image of ZW-MFNPs and ZW-MNPs. ZW-MNPs were fabricated as a reference for magnetic resonance imaging.

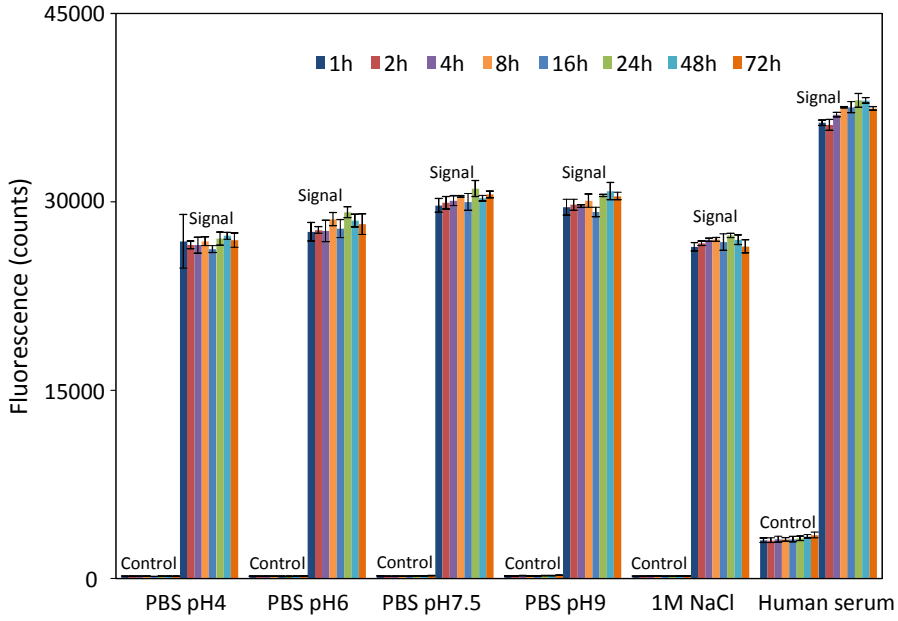

Figure 5. Fluorescence stability of ZW-MFNPs in PBS pH 4-9 solutions supplied with 5%FBS, a 1M NaCl-5%FBS, and human serum over hours at 37 °C – the fluorescence stability indicates the colloidal stability of MFNPs in the aqueous solutions.

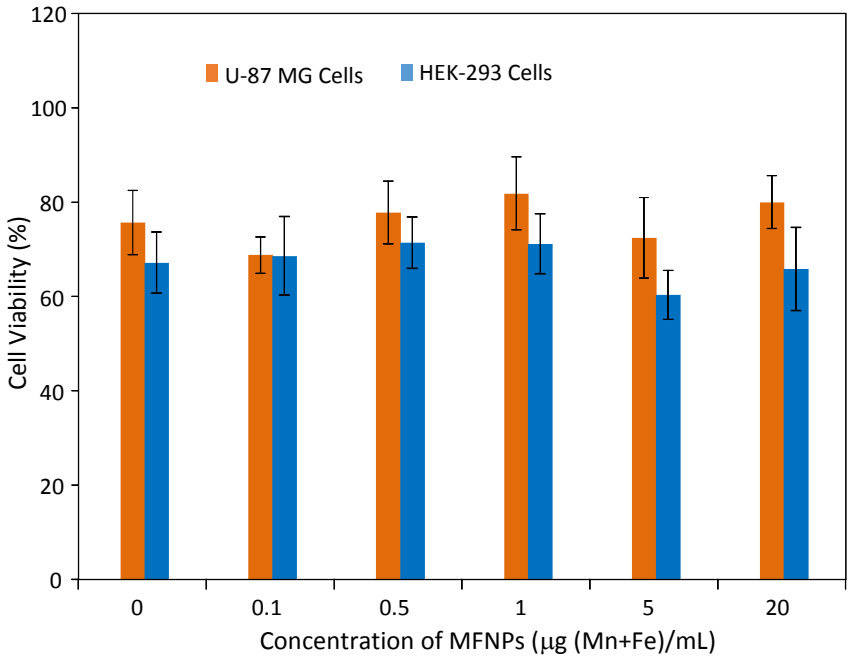

Figure 6. Cell viability of U-87 MG cell and HEK-293 cells treated with ZW-MFNPs at difference concentrations over 24 hours

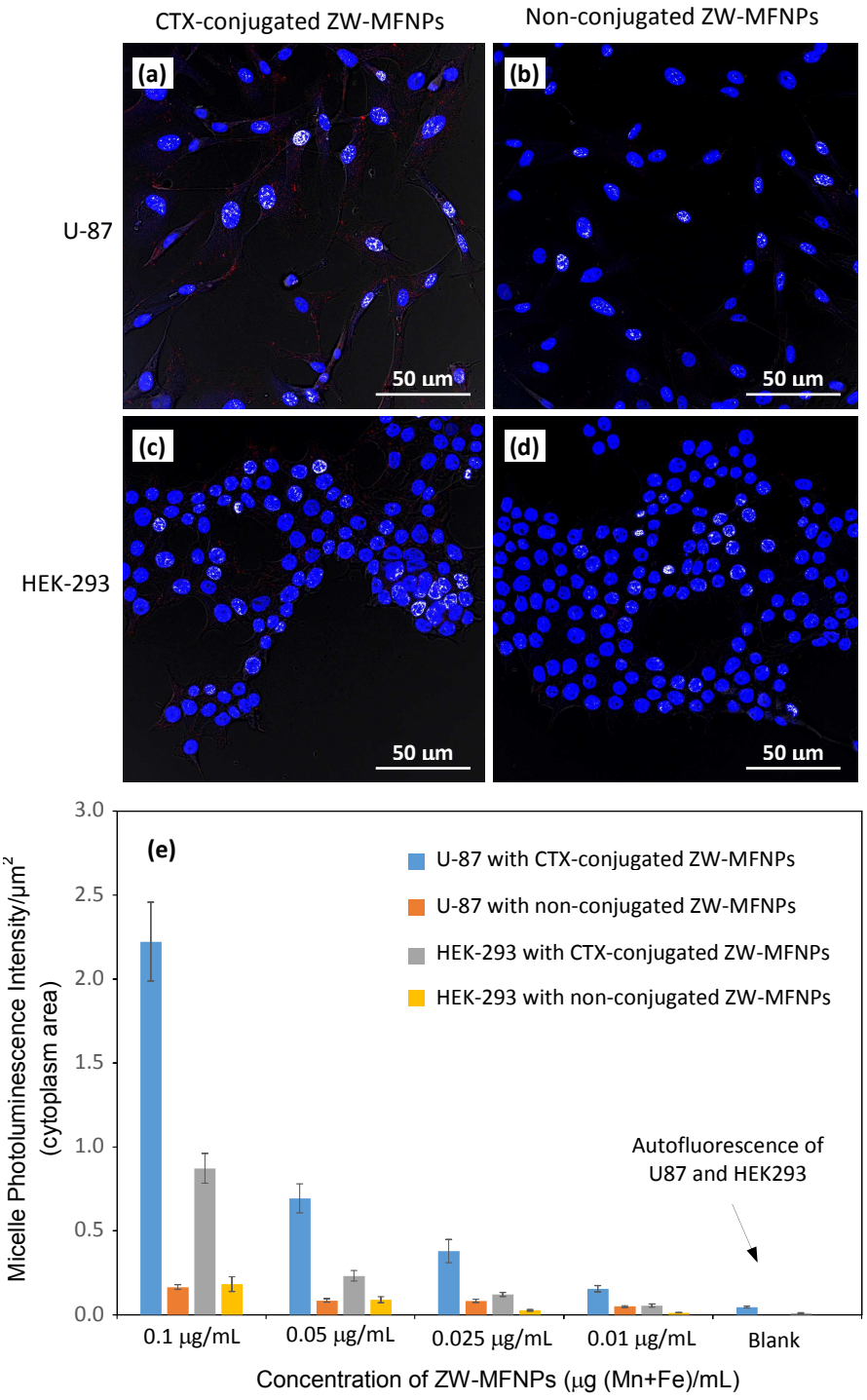

Figure 7. (a-d) Overlaid confocal images demonstrating the cellular uptake/internalization of CTX- and non-conjugated ZW-MFNPs under the same concentration of particles (0.1 μg (Mn+Fe)/mL) by U-87 and HEK-293; (e) Fluorescent intensity per unit area of cytoplasm for U-87 and HEK-293 cells incubated with CTX- and non-conjugated ZW-MFNPs with different concentrations. All *p* values for each comparison are less than 0.01.

Graphical Abstract:

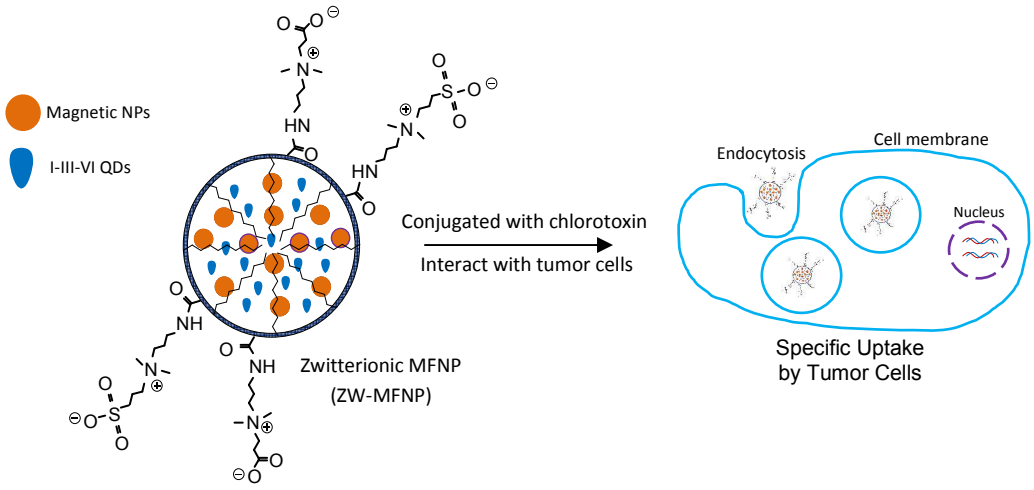

Zwitterionic magnetofluorescent nanoparticles (ZW-MFNPs) were prepared, characterized, and applied for specific tumor cell targeting.